Journal of Physics:
Conference Series

PAPER • **OPEN ACCESS**

Measuring Urban Heat Island Indicators from Surface Temperature Using Spatial Techniques

To cite this article: Yusra K. H. Moussa *et al* 2025 *J. Phys.: Conf. Ser.* **3028** 012051

Measuring Urban Heat Island Indicators from Surface Temperature Using Spatial Techniques

Yusra K. H. Moussa[1], Ahmed Asaad Zaeen [2], Hala A. Jasim [3], Mohammed I. Abd-almajied [4,] Eman H. Khudhair [5] Bushra K.H. Al-Maiyaly[6]

[1,3,4] Department of Remote Sensing and GIS, College of Science, University of Baghdad, Baghdad, Iraq

[2] Remote Sensing Unit, College of Science, University of Baghdad, Baghdad, Iraq.

[5] Department of Computer Science, College of Science, University of Baghdad, Baghdad, Iraq.

[6] Department of Physics, College of Education For Pure Science (Ibn Al-Haitham), University of Baghdad, Baghdad, Iraq

yosra.k@sc.uobaghdad.edu.iq.

boshra.k.h@ihcoedu.uobaghdad.edu.iq

Abstract. Using remote sensing technology and modeling methodologies to monitor changes in land surface temperature (LST) and urban heat islands (UHI) has become an essential reference for making decisions on sustainable land use. This study estimates LST and UHI in Salah al-din Province to contribute to land management, Urban planning, or climate resilience in the region; as a result of environmental changes in recent years, LANDSAT Satellite Imagery from 2014- 2024 was implemented to estimate the LST and UHI indexes in Salah al-din Province, ArcGIS 10.7 was use to calculate the indices, and The normalized mean vegetation index (NDVI) was calculated as it is closely related to extracting (LST & UHI) indices. Results confirmed that extracting the vegetation index, atmospheric radiation, brightness temperature of the satellite, and earth's surface emissivity from (Landsat-8) bands and processing them on ArcGIS facilitates the estimation of each of (LST and UHI) indexes. Results showed that (UHI) forms a complete correlation with (LST). The correlation coefficient in 2014 and 2024.

Keywords: Landsat 8, ArcGIS, normalized difference vegetation index (NDVI), land surface temperature (LST), and urban heat islands (UHI).

1. Introduction

Continued urbanization has many harmful influences, such as (UHI). Buildings within cities absorb sunlight and then re-radiate it, resulting in warmer surface temperatures than those around rural places. An investigation by [1] emphasizes the significance of satellite data processing, especially vegetation indices, in evaluating differences in Iraq's land cover. Their work examined the climatic factors' impacts on crop yield, especially temperature/ rainfall. They highlighted the exposure of rainfed growers to climate change, mainly shifts in rainfall customs and rising temperatures. Differences in rainfall and temperature customs due to climate change are consulted regarding their damaging consequences on plants. They noticed high humidity suggesting obstacles for agribusiness in Iraq [2]. Attention is drawn to the increasing presence of impermeable surfaces, which causes urban areas to change their surface radiation, humidity, and temperature. Furthermore, the drivers of the urban island phenomenon (UHI) are detailed by the expansion of urban structures, manufactured surfaces with high susceptibility to absorbing

solar radiation, shrinking areas covered by vegetation, heat generated by human activities, and atmospheric pollution [3-5].
A UHI includes financial/environmental disadvantages: more power necessities, pollution, reduced air quality [6], and health problems such as higher mortality rates and lower thermal comfort rates [7-8].
Defining a UHI's power and spatial distribution makes it achievable to display geographic place of the (UHI) related hazards [9]. An LST has employed indices to assess the UHI [10-12] while realized that land cover classes influence the relationship (UHI/heat), while the UHI power plant is more extensive in heat in more urbanized regions [13], investigated the landscape in urban places. They emphasized the diverse contributing aspects: recreational actions, and random urbanization leading to raised LST & UHI power due to human actions. This work emphasizes the critical necessity of evaluating landscape fragmentationm, It employs possible alternative strategies with multispectral imagery to evaluate urban growth by examining landscape fragmentation, not by employing traditional, not cost effective techniques inhibited by time restrictions[14]. Their novel technique includes spatial an original method to evaluate future urban growth pathways, supplying valuable data for decision-making [15, 16]. Because urban growth seriously influences a UHI, the temperature of the previously built-up areas tends to improve with new urban expansions. [17] noticed that an increase in the impenetrable surface and a reduction in vegetated land resulted in an LST growth in the investigation region. [18] documented the cooling impact of urban green areas while saying the significance of landscape arrangement and composition. Thus, many UHI mitigation policies concentrate on reducing the negative impacts of a UHI and enhancing the quality of life while raising vegetation in urban spaces [19]. Likewise, [20] highlighted that urban green areas could be UHI mitigation, while urban active zones are necessary for various planning techniques for green areas. Vegetation has a cooling impact due to its connection to the earth's albedo/surface temperature [21, 22]. Thus, some investigations indicate that the more comprehensive vegetation cover, the more sufficient urban cooling [23]. This study aims to evaluate the (LST, UHI, NDVI) using Landsat images, leading to sustainable land management and urban planning in Salah al-din.

2. Materials and Methods

2.1. Study area

Salah al-Din province is a strategic area characterized by its geographical location and the effects of continental climate; located in the Mesopotamian plain in Iraq, 160 km north of Baghdad, the capital; an average elevation of 50 m above the sea. It borders Nineveh to the north, Diyala to the east, Anbar to the west, and Baghdad and Babil to the south. Salah al-Din extends between latitudes 33.5° and 35° north and longitudes 43° and 44.5° east and occupies an area of about 24,751 km².
Salah al-Din Province's climate is semi-arid, with temperatures reaching approximately 45° Celsius during the summer, dropping below zero degrees in the winter, and limited rainfall rates [24]. The nature of the climate depends on the geographical location and the effects of air currents coming from the Western Desert and the Iranian Plateau region. The topography plays an important role in climate change, as the region includes extended plains with some low elevations and several valleys and water bodies that contribute to the daily and seasonal temperature variation [25]. The province is witnessing environmental changes related to global warming and rapid urban expansion, leading to significant changes in vegetation cover and water resources. According to the article, the application of remote sensing techniques showed a decrease in vegetation cover at clear rates because of human pressures and climate change [26, 27]. Climate change and vegetation cover studies can help develop environmental sustainability policies to improve natural resource management and reduce the effects of desertification. Recent research indicates the importance of geographic information systems (GIS) in assessing land cover dynamics and identifying

Journal of Physics: Conference Series **3028** (2025) 012051 doi:10.1088/1742-6596/3028/1/012051

areas most affected by climate change [28]. Figure 1 below shows the location of Salah al-Din Province in Iraq.

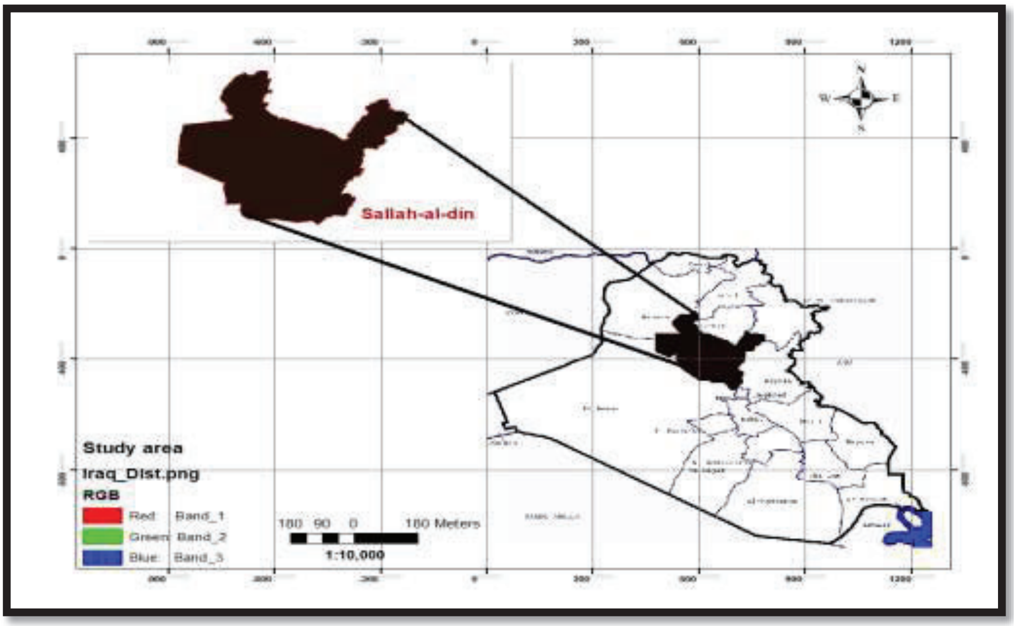

Figure 1. The Study Area

2.2. Data sets and methods:

Thermal infrared remote sensing data from Landsat-8 OLI/TIRS (bands 10, 11) was adopted from USGS website (USGS, http://earthexplorer.usgs.gov) [29]. Satellite images of Salah Al-Din were captured on August 12, 2014, and August 16, 2024. ArcMap 10.7 was used to correct the data for atmospheric distortions and extract the boundaries of the study area. The shapefile data was adopted at a map scale of (1:1,300,000). Landsat 8 has a thermal infrared sensor (TIRS) with a resolution of 100 meters, includes bands (10 and 11), and is used to collect thermal data. It was used to collect LST data in which the stray light effect is sufficient in band 10 and band 11 to make the data useful across a wide range of applications. The Operational Land Imager (OLI) with bands (1-9) and a resolution of 30 meters is used to collect non-thermal data [30]. Cloud-free data from 2014 to 2024 was selected to avoid cloud effects. The corrected Landsat data were used to generate the NDVI, LST, and UHI maps, and then the relationship between them was investigated. Figure 2 shows a schematic of how the STI and UHI were evaluated.

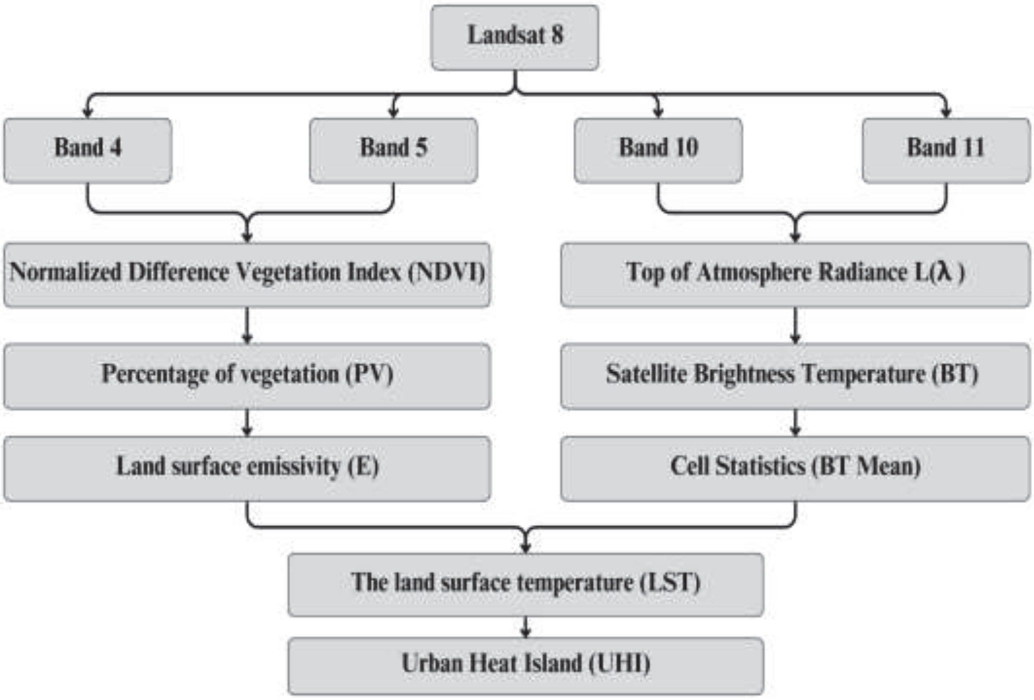

Figure 2. Graph showing how the LST and UHI are evaluated

2.3. Satellite Imagery Acquisition:

Satellite images were obtained from the USGS Earth Explorer database. Figure 3 shows the Landsat images of Salah al-Din Governorate in 2014 and 2024 with a ground resolution of 30 m from the sensor Landsat 8 carries Operational Land Image (OLI)/TIRS sensors from Collection 2/ Level 1, Table 1.

Table 1. Information on the images of Landsat were used in the study

NO.	Launched Date	cloud cover	Path/Row	Satellite Image	Image level	Sensor Type	Source
1	12/08/2014	0.00	168/38	LANDSAT-8	Collection 2/ Level 1	Operational Land Image (OLI)/TIRS	USGS Earth Explorer Database
2	12/08/2014	0.00	169/38				
3	12/08/2014	0.08	169/37				
4	16/08/2024	0.00	169/38				
5	16/08/2024	0.00	169/37				
6	16/08/2024	0.00	168/38				

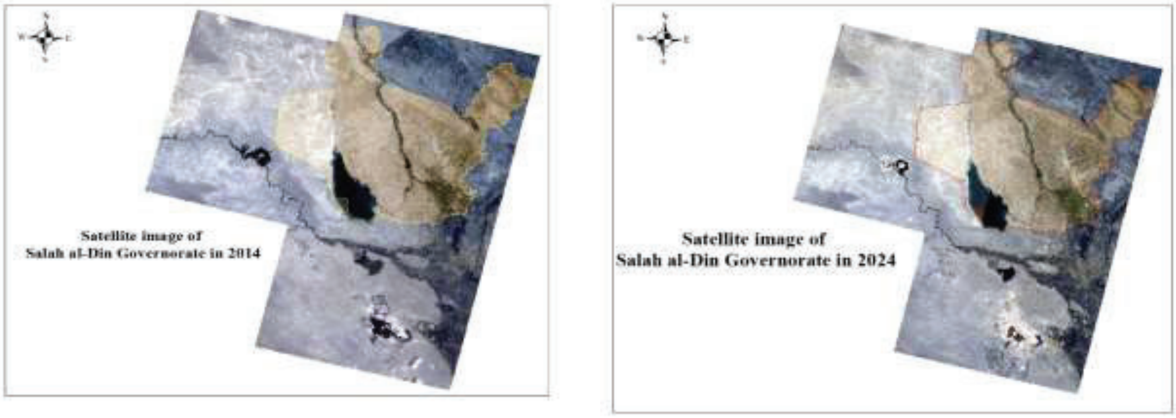

Figure 3. Landsat images of Salah al-Din Governorate in 2014 and 2024

2.4. Methodology:
Landsat 8 satellite image was obtained from USGS website, earthen plorer.usgs.gov; thermal bands (10 and 11) and Bands (4 and 5) were used and processed using ArcGIS 10.7. To ensure the effectiveness of the study, the following criteria will be considered:

1- The NDVI was used to determine density and health of vegetation based on the reflectivity of the Earth's surface to near-infrared (NIR) and red (RED) light. Equation (1) was used to compute the NDVI [31].

$$NDVI = \frac{\text{NIR} + \text{RED}}{\text{NIR} - \text{RED}} \dots\dots\dots\dots\dots\dots (1)$$

NIR and RED were calculated from Landsat 8, Band 5, and 4.

Table 2. Landsat band information

Source	Bands	Wavelength(μm)
Landsat8 (OLI)	4 (Red)	0.636-0.673
	5 (NIR)	0.851-0.879

2- The percentage of vegetation (PV) used to calculate land surface thermal radiation (LSE) is between 0 and 1, indicating the vegetation density in a pixel. PV is calculated using Equation (2):

$$PV = \left(\frac{NDVI - NDVI_{min}}{NDVI_{max} - NDVI_{min}}\right)^2 \dots\dots\dots\dots (2)$$

Where: NDVI represents the vegetation index value calculated for each pixel.
$NDVI_{max}$: The highest NDVI value, usually close to 1 for dense vegetation.
$NDVI_{min}$: The lowest NDVI value, usually close to 0 or negative for bare soil and water.

PV value was based on normalizing the NDVI values to 0 and 1, determining each pixel's vegetation density. The resulting value is squared to contrast dense and sparse vegetation areas. If the NDVI is close to the upper limit, the PV approaches 1, indicating dense vegetation, and if it is

Journal of Physics: Conference Series **3028** (2025) 012051 doi:10.1088/1742-6596/3028/1/012051

close to the lower limit, the PV approaches 0, indicating the presence of soil or water. This value calculates the land surface thermal radiation (LSE), improving the accuracy of LST's climate and agricultural studies.

3- Land surface thermal radiation (LSE), or (E) for short, is a measure of surface that emits heat radiation compared to an ideal black body at the same temperature. LSE improves the accuracy of LST calculations. It is determined based on vegetation cover using the NDVI index, where PV is first calculated by normalizing the NDVI between its maximum and minimum values, and by using Equation (3), the value of LSE is calculated [32].

$$\mathrm{E} = 0.004 \times \mathrm{PV} + 0.986 \ldots\ldots\ldots\ldots.(3)$$

Different surfaces reflect different radiances, with water and dry soil having low radiances (~0.92) while dense vegetation has high radiances (~0.98). LSE is essential for accurate LST calculations, especially in climate studies, drought analysis, and UHI, as it helps correct the effects of different land surface characteristics on satellite-measured temperatures.

4- The LST is calculated using Equation (4), measured in Kelvin or Celsius (32).

$$LST = \frac{BT}{\ln(E) * \left(\frac{\lambda * BT}{C2}\right) + 1} \ldots\ldots\ldots\ldots\ldots.(4)$$

Brightness Temperature (BT) is the spectral brightness temperature measured by the satellite at the top of the atmosphere, and it can be calculated using Equation (5) [33, 34].

$$BT = \frac{K2}{\ln(\frac{K1}{L(\lambda)} + 1)} - 273.15 \ldots\ldots\ldots\ldots\ldots\ldots\ldots\ldots.(5)$$

Where K 1and K2 are Landsat 8 constants equal to 774.8853 and 1321.0789, respectively, the wavelength (λ) of thermal radiation equals (10.8) µm. BT and λ are calculated from Landsat 8 Band 10 [35].

C_2: Thermal irradiance constant equal to (14388) MK, calculated using Equation (6):

$$C_2 = \frac{h * C}{S} \ldots\ldots\ldots\ldots\ldots..(6)$$

h is Planck's constant,(6.626×10^{-34} measured with J/s),
C is the speed of light (2.998×10^{-8} m/s),
S is Boltzmann's constant ($1.38 * 10^{-23}$ J/K).

5- The (UHI) Index was used to identify areas most at risk of atmospheric anomalies. Surface temperature normalization methods were used through the following equation: (7) [35].

$$UHI = \frac{(LST - LST_m)}{(LST_{sd})} \ldots\ldots\ldots\ldots\ldots\ldots\ldots..(7)$$

Where: LST_m = mean of the land surface temperature of the study area, and LST_{sd} = Standard Deviation.

Journal of Physics: Conference Series **3028** (2025) 012051 doi:10.1088/1742-6596/3028/1/012051

3. Results and discussions

3.1. Normalized Difference Vegetation Index (NDVI):
Bands 4 and 5 of the Landsat image were used to calculate this index; it indicates areas where vegetation is present. NDVI values showed a clear decline between 2014 and 2024, as shown in Table 4, figure 4.

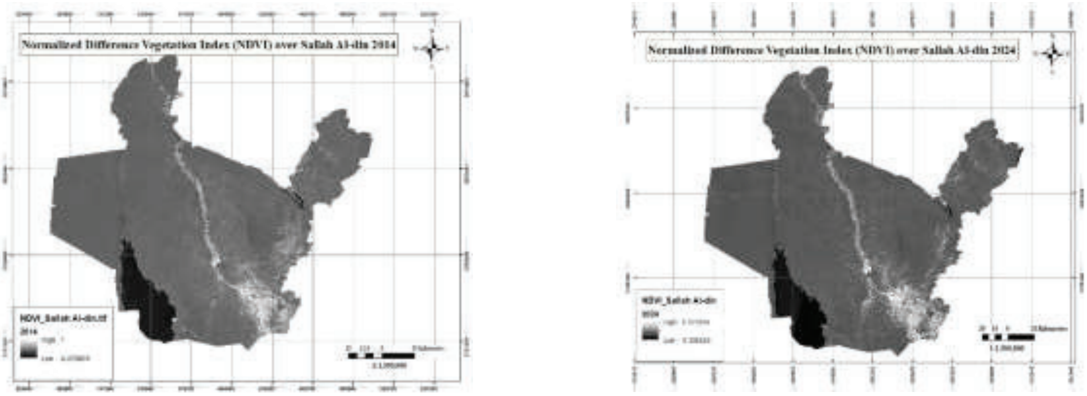

Figure 4. Standardized Vegetation Index map for 2014 and 2024

The percentage of shrub area decreased from (6.3 - 1.9%), equivalent to (1.0874 km2), and the percentage of dense plants decreased from (1.2 - 0.4%), equivalent to (0.196 km2), while the urban cover area expanded by (1.0272 km2), as the percentage increased from (89.2 - 93.4%) between 2014 and 2024. as shown in Table 3, figure 5.

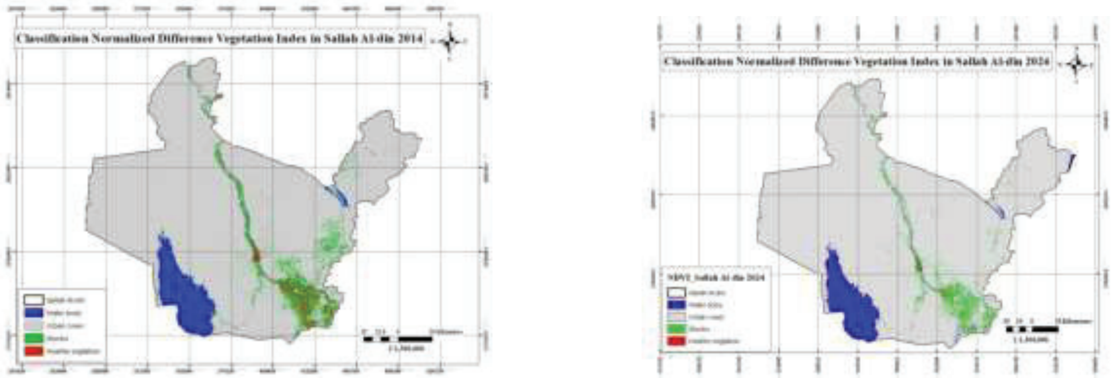

Figure 5. Classification Vegetation map for 2014 and 2024

Table 3. Classification Vegetation for 2014 and 2024

Class	2014		2024	
	Area%	Area_km2	Area%	Area_km2
Waterbodies	3.175534	0.785976	4.208179	1.041566
Urben caver	89.2798	22.09764	93.43011	23.12489
Shurbs	6.340567	1.569354	1.947086	0.481923
Heaithy vegtation	1.2041	0.298027	0.414627	0.102624
Total	100%	24.751	100%	24.751

Journal of Physics: Conference Series **3028** (2025) 012051 doi:10.1088/1742-6596/3028/1/012051

3.2. Land Surface Temperature (LST):

It represents the surface temperatures of each element within a pixel. The LST of the study area was determined using satellite data. LST maps of the research area were generated in ten years from 2014 to 2024, using the above equations to analyze data from Landsat-8 Thermal Band 10 in ArcGIS 10.7. This indicates in the maps of Salah al-din province that the surface temperature ranges become higher when comparing the years 2014 and 2024, and high surface temperatures were observed in the city's interior areas in the east and northeast of the study area due to urban expansion and the presence of some exposed areas devoid of vegetation. In contrast, low surface temperatures were found in the surrounding water and vegetation concentration areas, figure 5. The values of LST witnessed a clear increase between 2014 and 2024, as shown in Table 4.

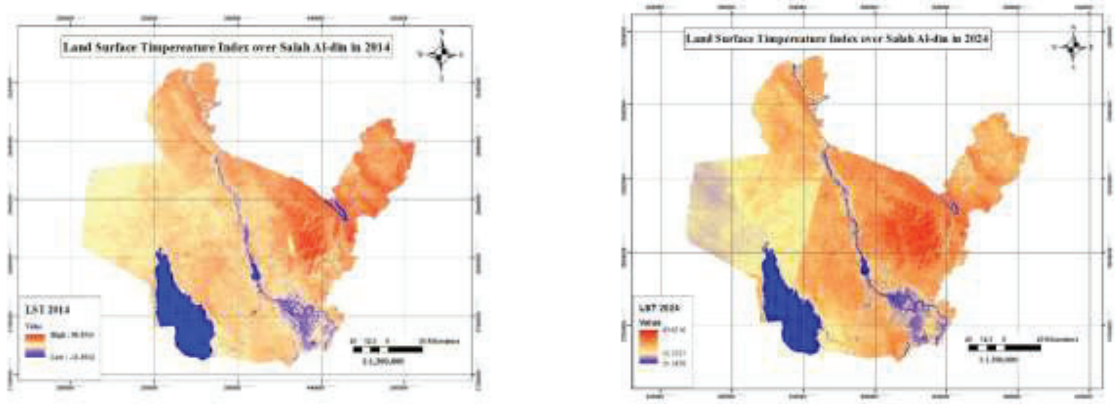

Figure 6. LST of Salah al-din province for the years 2014 and 2024

3.3. Urban Heat Island Index (UHI)

Figure 6 shows the UHI levels for 2014 and 2024. UHI maps were created for the research area. It was found that inland areas have higher levels of temperature compared to other areas close to bodies of water and the presence of plants. The values of UHI witnessed a clear increase between 2014 and 2024, as shown in Table 4.

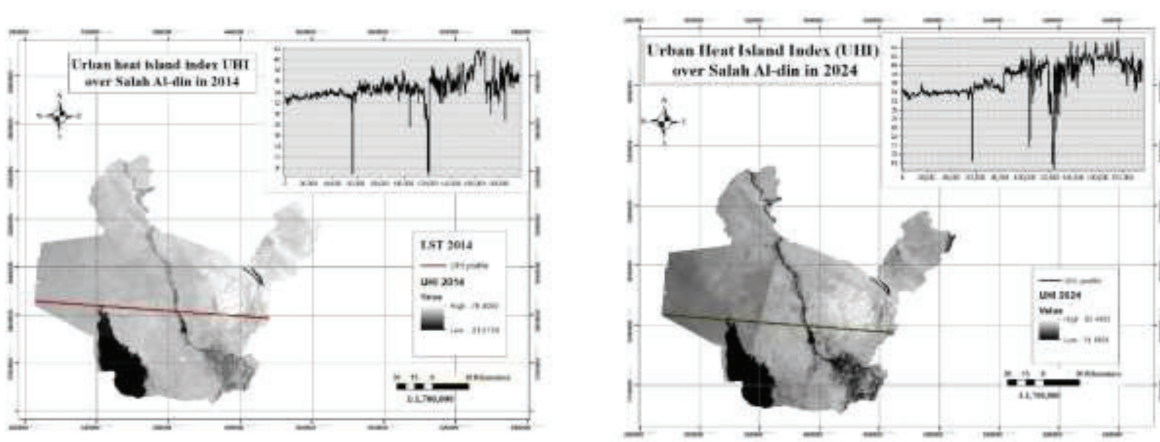

Figure 7. UHI Index of Salah al-din Province for the years 2014 and 2024

Journal of Physics: Conference Series **3028** (2025) 012051 doi:10.1088/1742-6596/3028/1/012051

Table 4. NDVI, LST, and UHI Indexes of Salah al-din Province for the years 2014 and 2024

Index	2014		2024	
	Max	Min	Max	Min
NDVI	1	-0.279809	0.572979	-0.306343
LST	86.4314	-11.4912	93.6516	24.3429
UHI	76.4069	-21.5156	83.4492	14.1405

This study examined the relationship between vegetation scatterplots (as measured by NDVI), LST, and UHI between 2014 and 2024. Figure 7 shows the linear relationship between UHI, LST, and NDVI in 2014 and 2024.

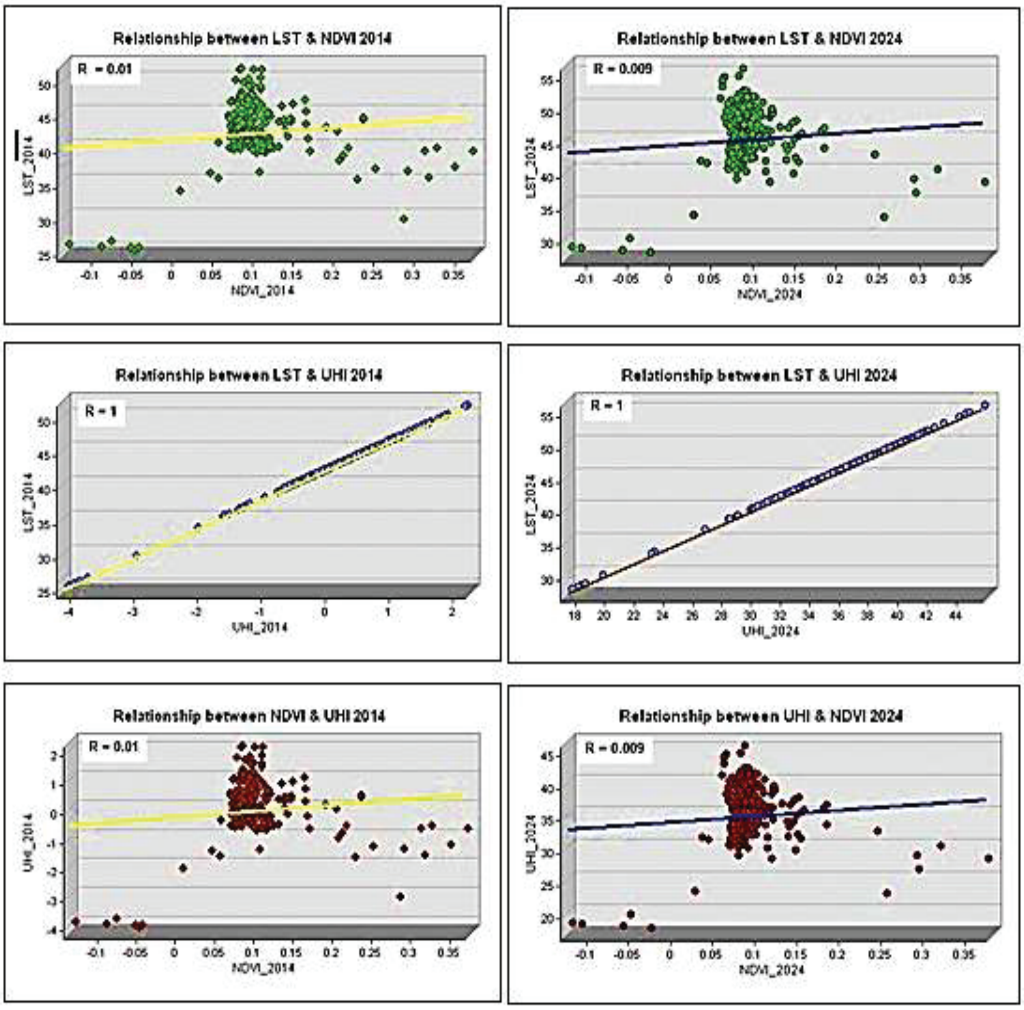

Figure 8. The relationship among (NDVI, UHI, LST) in 2014 and 2024

Journal of Physics: Conference Series **3028** (2025) 012051 doi:10.1088/1742-6596/3028/1/012051

4. Conclusion

The relationship between LST and UHI index can be estimated using (remote sensing and GIS) techniques, and variance between these climatic factors can be determined over ten years. The results show a very weak the positive correlation between (LST and NDVI) in 2014, with a correlation coefficient of 0.01, and the relationship weakened over the ten years until it became in 2024 with a correlation coefficient of 0.009, meaning that LST increases as NDVI values decrease. The results also showed a strong correlation between LST and UHI, with a correlation coefficient 1 in 2014 and 2024. A weak correlation exists between (urban heat island index UHI) and (natural vegetation index NDVI) in 2014. We see that the correlation coefficient is about 0.01, and the relationship trended over the ten years until 2024, with a correlation coefficient of 0.009. The identification of these two important environmental factors facilitates the process of environmental monitoring: the distribution of temperature conditions and heat islands in the study area, and their integration allows for a drought monitoring system that can be used in the fields of urban planning, agriculture and water resources management in the study area. The optimal solution to mitigate the effects of urban heat islands is to expand vegetation cover, which is a key strategy for achieving urban sustainability.

5. Future Studies

The relationship between urban expansion, (LST), and (UHI). Future studies can expand to include other cities, thus enabling us to solve urban heat island problems.

References

[1] Jabal ZK, Khayyun TS, Alwan IA 2022 Impact of climate change on crops productivity using MODIS-NDVI time series. *Civil Engineering Journal* **8**(6):1136-56.

[2] Tian P, Li J, Cao L, Pu R, Wang Z, Zhang H, et al. 2021 Assessing spatiotemporal characteristics of urban heat islands from the perspective of an urban expansion and green infrastructure. *Sustainable Cities and Society* 74:103208.

[3] Aleksandrowicz O, Vuckovic M, Kiesel K, Mahdavi A 2017 Current trends in urban heat island mitigation research: Observations based on a comprehensive research repository. *Urban Climate* **21**:1-26.

[4] Palme M, Inostroza L, Villacreses G, Lobato-Cordero A, Carrasco C 2017 From urban climate to energy consumption. Enhancing building performance simulation by including the urban heat island effect. *Energy and buildings* **145**:107-20.

[5] He B-J 2019 Towards the next generation of green building for urban heat island mitigation: Zero UHI impact building. *Sustainable Cities and Society* **50**:101647.

[6] Lowe SA 2016 An energy and mortality impact assessment of the urban heat island in the US. Environmental Impact *Assessment Review* **56**:139-44.

[7] Venter ZS, Krog NH, Barton DN 2020 Linking green infrastructure to urban heat and human health risk mitigation in Oslo, Norway. *Science of the Total Environment* **709**:136193.

[8] Li X, Zhou Y, Yu S, Jia G, Li H, Li W 2019 Urban heat island impacts on building energy consumption: A review of approaches and findings. *Energy* **174**:407-19.

[9] Singh R, Grover A **2015** Spatial correlations of changing land use, surface temperature (UHI) and NDVI in Delhi using Landsat satellite images. Urban development challenges, risks and resilience in Asian megacities **54**:83-97.

[10] A. K. Taloor, D. S. Manhas, G. C. Kothyari 2021 Retrieval of land surface temperature, normalized difference moisture index, normalized difference water index of the Ravi basin using Landsat data. *Appl Comput Geosci* **9**(100051.).

[11] Sun T, Sun R, Chen L 2020 The trend inconsistency between land surface temperature and near-surface air temperature in assessing urban heat island effects. *Remote sensing* **12**(8):1271.
[12] Zou Z, Yan C, Yu L, Jiang X, Ding J, Qin L, et al. 2021 Impacts of land use/land cover types on interactions between urban heat island effects and heat waves. *Building and Environment* **204**:108138.
[13] Kadhim N, Ismael NT, Kadhim NM 2022 Urban landscape fragmentation as an indicator of urban expansion using sentinel-2 imageries. *Civil Engineering Journal* **8**(9):1799-814.
[14] Moussa YKH, Alwehab AA 2023 Evaluation of Climate Change Indicators for Bagdad City Using Remote Sensing Technology. *Iraqi Journal of Science* **64**(8):5190-201.
[15] Moussa YKH, Alwehab AA 2024 Measuring Changes in Temperature Rates due to Urban Expansion in Selected Municipalities of Baghdad using GIS Technology. *Iraqi Journal of Physics* **22**(3):126-38.
[16] Wang J, Huang B, Fu D, Atkinson PM, Zhang X 2016 Response of urban heat island to future urban expansion over the Beijing–Tianjin–Hebei metropolitan area. A*pplied Geography* **70**:26-36.
[17] Rousta I, Sarif MO, Gupta RD, Olafsson H, Ranagalage M, Murayama Y, et al. 2018 Spatiotemporal analysis of land use/land cover and its effects on surface urban heat island using Landsat data: A case study of Metropolitan City Tehran (1988–2018). *Sustainability* **10**(12):4433.
[18] Yao L, Li T, Xu M, Xu Y 2020 How the landscape features of urban green space impact seasonal land surface temperatures at a city-block-scale: An urban heat island study in Beijing, China. *Urban Forestry & Urban Greening* **52**:126704.
[19] Arghavani S, Malakooti H, Bidokhti A-AAA 2020 Numerical assessment of the urban green space scenarios on urban heat island and thermal comfort level in Tehran Metropolis. *Journal of cleaner production*. **261**:121183.
[20] Ke X, Men H, Zhou T, Li Z, Zhu F 2021 Variance of the impact of urban green space on the urban heat island effect among different urban functional zones: A case study in Wuhan. *Urban Forestry & Urban Greening* **62**:127159.
[21] Adeyeri O, Akinsanola A, Ishola K 2017 Investigating surface urban heat island characteristics over Abuja, Nigeria: Relationship between land surface temperature and multiple vegetation indices. Remote Sensing Applications: *Society and Environment* **7**:57-68.
[22] Moussa YKH, Alwehab AA 2022 The Urban Expansion Impact on Climate Change for the City of Baghdad. *Iraqi Journal of Science* **63**(11):5072-85.
[23] Al-Saadi LM, Jaber SH, Al-Jiboori MH 2020 Variation of urban vegetation cover and its impact on minimum and maximum heat islands. *Urban Climate* **34**:100707.
[24] AL-Bakri NWaM 2023 Investigating The Relationship between Land Surface Temperature (LST) and The Expansion of Built-up Land, A case Study of Baghdad, Iraq **64**(12):6648–61.
[25] Al-Turaihi JHA-Z, and J. K. Mani 2022 Vegetation Cover Variations in Central Iraq by Using GIS and Remote Sensing Data. I*raqi Geological Journal* **55**(1F):122-3.
[26] Al-Zubaydi N and H. A. Al-A 2024 Hydrological Study of the Great Musaiyab Project Babylon Governorate in Middle of Iraq. IOP Conference Series: *Earth and Environmental Science* **1371**(8):082005.
[27] Taktikou GB, G. Papaioannou, and P 2016 Prediction of Soil Moisture from Remote Sensing Data. Procedia Engineering, Elsevier Ltd **162**:309–16.
[28] Richards JA, & Richards, J. A,. Remote sensing digital image analysis Berlin/Heidelberg, Germany: *Springer*. 2022;5:256-8.
[29] Missions UL 2019 Using the USGS Landsat Level-1 Data Product. USGS Science for a Changing World. Available online: [Available from: https://www. USGS. gov/landsat-missions/using-usgs-landsat-level-1-data-product

[30] Tajudin NY, Ali D. M, and Adnan N A 2021 Soil moisture index estimation from Landsat 8 images for prediction and monitoring landslide occurrences in Ulu Kelang, Selangor, Malaysia. *International Journal of Electrical and Computer Engineering* **11**(3):2101-8.
[31] Sobrino J 2004 Land surface temperature retrieval from LANDSAT TM 5. *Remote Sensing Environmental* **90**(4):434-40.
[32] Pal T and Pant L 2021 Thapa. Hydrochemical assessment of the Beeshazar and associated lakes in Central Nepal. SN *Applied Sciences* **3**(38):1-13.
[33] Pal K, Chalaune T, Pant R, Thapa L 2021 Hydrochemical assessment of the Beeshazar and associated lakes in Central Nepal. SN *Applied Sciences* **3**(38).
[34] Avdan U, Kaplan G 2016 Algorithm for automated mapping of land surface temperature using LANDSAT 8 satellite data. Hindawi Publishing Corporation / *Journal of Sensors* (**2**).
[35] Negash DA, Getahun K, Gebre SL 2024. Seasonal spatial-temporal variation of the urban heat island effect in Bahir Dar city using land surface temperature data. *Ethiop J Appl Sci Technol* **15**(1).